NASA Contractor Report 185132

Mathematical Modeling and Analysis of Heat Pipe Start-Up From the Frozen State

Jong Hoon Jang and Amir Faghri
Wright State University
Dayton, Ohio

and

Won Soon Chang and Edward T. Mahefkey
Wright Research and Development Center
Wright-Patterson AFB, Ohio

August 1989

Prepared for
Lewis Research Center
Under Contract F336 15-88-C-2820

National Aeronautics and
Space Administration

MATHEMATICAL MODELING AND ANALYSIS OF HEAT PIPE START–UP FROM THE FROZEN STATE

by

Jong Hoon Jang[+] and Amir Faghri[*]
Department of Mechanical and Materials Engineering
Wright State University
Dayton, Ohio 45435

and

Won Soon Chang and Edward T. Mahefkey
Wright Research and Development Center
Wright–Patterson AFB, OH 45433

ABSTRACT

The start–up process of a frozen heat pipe is described and a complete mathematical model for the start–up of the frozen heat pipe is developed based on the existing experimental data, which is simplified and solved numerically. The two–dimensional transient model for the wall and wick is coupled with the one–dimensional transient model for the vapor flow when vaporization and condensation occur at the interface. A parametric study is performed to examine the effect of the boundary specification at the surface of the outer wall on the successful start–up from the frozen state. For successful start–up, the boundary specification at the outer wall surface must melt the working substance in the condenser before dry–out takes place in the evaporator.

NOMENCLATURE

c_p	specific heat at constant pressure, J/kg–K
c_v	specific heat at constant volume, J/kg–K
D	diameter of the vapor space, m
E	total energy of the vapor per unit volume, $\rho [c_v T_v + 1/2 (U_v^2 + V_v^2)]$
f	friction coefficient at the wall, $\tau/\rho U_v^2$
h	enthalpy, J/kg
h_c	heat transfer coefficient, $W/m^2 - K$
h_{fv}	latent heat of vaporization, J/kg
$H_{s\ell}$	latent heat of melting per unit volume, J/m^3
k	permeability of the wick structure, m^2
K	thermal conductivity, W/m–K
L	length of the heat pipe, m
$\dot{m}_0$	rate of evaporation or condensation per unit area, $kg/m^2–s$
M	molecular weight, kg/Kmol
n	unit outward normal direction
P	pressure, N/m^2
q	heat flux, W/m^2
q′	new heat flux, W/m^2
q^n	new guessed heat flux, W/m^2
P_{cr}	reference pressure for the Clausius–Clapeyron relationship, N/m^2
r	coordinate in the radial direction
r_c	effective capillary radius, m
r_p	radius of curvature of the meniscus, m
Δr	radial distance between nodes, m
R_u	universal gas constant, KJ/Kmol–K
R_v	radius of the vapor space, m
R_w	inner radius of the heat pipe wall, m
$\vec{S}$	interface position in vector, m
t	time, s
T	temperature, K
T_c	reference temperature for convection, K
T_{cr}	reference temperature for the Clausius–Clapeyron relationship, K
T_m	melting temperature, K
T_r	reference temperature for radiation, K
T_s	saturation temperature, K
T_{j-1}	temperature at node j–1 in the radial direction in the wick region, K
T_j	temperature at last node near liquid–vapor interface in the radial direction in the wick region, K
T^*	transition temperature, K

[+]Currently with Sverdrup Technology, Inc., NASA Lewis Research Center Group, Cleveland, Ohio 44135.

[*]Professor.

ΔT small finite temperature interval around T_m to define mushy zone, K
U axial velocity, m/s
V radial velocity, m/s
x coordinate in the axial direction

GREEK SYMBOLS
α relaxation factor
$\delta(T - T_m)$ Dirac function
ϵ porosity
θ contact angle of the liquid, deg
λ length of mean free path, m
μ dynamic viscosity, N–s/m^2
ν kinematic viscosity, m^2/s
ξ emissivity
ρ density, kg/m^3
σ Stefan–Boltzmann constant, W/(m^2–K^4)
τ shear stress
ω surface tension, N/m

SUBSCRIPTS
ll working substance in the liquid state in the wick
fs working substance in the solid state in the wick
l liquid where there is liquid motion in the wick
le wick region where the working substance is in the liquid state
me wick region where the working substance is in the mushy state
o properties at the liquid–vapor interface
s wick structure material
se wick region where the working substance is in the solid state
v vapor state
w properties at the heat pipe wall

INTRODUCTION

The demand for an effective thermal management device for high temperature applications such as cooling the leading edges of reentry vehicles and hypersonic aircraft, and a space–based power station stimulates the study of the start–up of frozen liquid–metal heat pipes. Also, the start–up of frozen low temperature heat pipes is important in applications such as heat pipe heat exchangers, cooling electronic equipment, and melting the snow and ice on roads and bridges.

Neal (1967) and Shlosinger (1968) performed the first experimental tests to study the start–up performance of low temperature heat pipes with the water initially frozen. Deverall et al. (1970) also made a series of tests with water and liquid metal heat pipes. Successful start–up from the frozen state was possible but was highly dependent on the heat rejection rate at the condenser. Tolubinsky et al. (1978) investigated the start–up characteristics of sodium and potassium heat pipes. Camarda (1977) investigated the performance of a sodium heat pipe cooling a leading edge. Start–up and shut–down of a 4 m long lithium heat pipe was studied experimentally by Merrigan et al. (1985, 1986). Ivanovskii et al. (1982) presented the vapor temperature distribution along the length of a sodium heat pipe during the start–up period. Three flow regimes in the condenser are described based on the vapor temperature: free molecular flow, intermediate, and continuum vapor flow. Unfortunately, the existing experimental data for the start–up period are in general not represented in the archival literature and lack sufficient information for comparison with numerical simulations.

Colwell et al. (1987) and Jang (1988) developed a simple mathematical model to predict the start–up behavior of a sodium heat pipe with a rectangular cross section from the frozen state. In the wall and wick structure, energy transport is described by the transient, two–dimensional heat conduction equation, and the phase change of the working substance is taken into account. In the vapor region, free molecular, choked and continuum flows are considered and one–dimensional, compressible quasi–steady state laminar flow is assumed. The numerical results obtained by using the finite element method are in agreement with experimental results given by Camarda (1977).

The liquid metal heat pipe operates not only at high temperatures but also the initial temperature may be ambient temperature. In this temperature range, the working substance may be in the solid state as well as the liquid and vapor states. In the vapor space, free molecular flow, continuum flow, sonic and supersonic flow may be encountered due to the extremely small density during the start–up of the heat pipe. These conditions may cause the failure of operation of the heat pipe and limit the performance of the heat pipe. Understanding the start–up behavior and transient performance of the high temperature heat pipe is therefore important and an efficient mathematical model is needed to predict this behavior.

The first part of this paper presents a complete mathematical model to describe the start–up behavior of the heat pipe from the frozen state. This model is then simplified to obtain numerical results. To the authors' knowledge, the analysis presented here is the only model that includes the effect of the transient vapor flow in the analysis of the start–up of a heat pipe from the frozen state. After the mathematical models are tested separately, the models are used for a parametric study of the start–up of frozen heat pipes.

DESCRIPTION OF HEAT PIPE START–UP

Previous experimental observations suggest the following sequence of events during heat pipe start–up from the frozen state. Initially, the working substance is in the solid state and the vapor density is extremely low, so that free molecular flow conditions prevail throughout the vapor space. The input heat flux over the evaporator increases the temperature and starts to melt the frozen substance in this region. Meanwhile, the heat transport from the heated zone to the adjacent pipe proceeds quite slowly via axial conduction through the heat pipe wall, working substance, and wick structure, while the heat transfer in the vapor is almost negligible. Thus, a large temperature gradient exists between the evaporator and condenser.

When energy is continuously added to the evaporator, the frozen working substance in the evaporator is melted, so that evaporation can take place at the liquid–vapor interface and the vapor density in this region is increased. The molecular mean free path in the heated region then becomes small compared to the diameter of the vapor passage and the continuum flow regime is established, while in the cooled zone the vapor is still in free molecular flow. In the continuum flow region, the vapor flows into the condenser section due to the large pressure gradient. During this stage, energy is mainly transferred as latent heat owing to vaporization in the heated zone, and condensation in the cooled zone in the vapor space where continuum flow is established. The temperature near the evaporator remains constant and the location of the temperature gradient moves toward the end of the condenser until continuum flow is established in the entire vapor space. Cotter (1967) also described this frontal start–up mode when the vapor density is so low and non–condensable gas does not exist in the vapor space.

In heat pipes with metallic working substances, the vapor densities are very small during the start–up even in the continuum flow region. Thus, even for relatively low values of heat input, sonic vapor velocities can be reached.

Also, the vapor flow in the heat pipe is quite similar to the flow in a converging–diverging nozzle due to the vapor addition in the evaporator and the vapor removal in the condenser (Dunn and Reay, 1982). Thus, the heat transfer through the vapor space may be limited by the choked flow condition, and supersonic vapor flow and a shock front may occur in the continuum flow region in the condenser. The maximum rate of heat transfer is limited by the sonic limit so that a high heat input in the evaporator causes the various types of start–up failure.

The start–up process continues until the frozen working substance is completely melted and the continuum flow regime reaches the end of the heat pipe, at which time liquid returning to the evaporator is sufficient for normal transient operation. Eventually, the heat pipe may reach a steady state condition. The start–up process of the liquid metal heat pipe from a frozen state may be divided into several distinct periods for convenience of analysis based on the status of the working substance and the behavior of the vapor flow.

1. In the first period, no phase change takes place in the entire region but the temperature near the heated region increases. The vapor flow is in the free molecular condition.
2. The working substance in the evaporator is in the liquid state, but evaporation does not occur at the liquid–vapor interface.
3. The liquid and solid states of the working substance exist simultaneously in the wick structure and vaporization of the working substance takes place at the liquid–vapor interface. In the vapor space, a region of continuum flow is established in the heated region and a continuum flow front moves toward the cooled end of the heat pipe. The vapor flow may be choked at the beginning of the condenser.
4. The working substance is completely melted but free molecular flow still exists in part of the vapor space.
5. Continuum flow exists over the entire heat pipe length in the vapor region but the heat pipe does not reach the steady state condition.
6. The heat pipe then reaches the steady state operation.

For low temperature heat pipes, the experimental results of the successful start–up from the frozen state are very rare. Deverall et al. (1970) successfully started a water heat pipe from the frozen state (208 K). The wall temperature distribution obtained is similar to that of high temperature heat pipes. The vapor temperature was not obtained, but the vapor density is relatively high even around the melting temperature. This means that the vapor velocity is very low so that choked flow and supersonic vapor velocities may not be encountered during start–up. Unlike high temperature heat pipes, experimental results show that the heat pipe becomes immediately active where the ice is melted, but there still is a large temperature gradient in the axial direction. The heat input at the evaporator should be low enough to return sufficient water into the evaporator for the successful start–up.

MATHEMATICAL FORMULATION

Consideration is given to the heat pipe wall, the wick structure with the working substance initially subcooled at a uniform temperature, and the vapor region. A schematic diagram of the physical model is shown in Fig. 1.

Heat Pipe Wall

In this region, the progress can be modeled by the heat conduction equation in a hollow cylinder. The governing equation are expressed as follows:

$$(\rho c_p)_w \frac{\partial T_w}{\partial t} = \frac{1}{r}\frac{\partial}{\partial r}\left[rK_w \frac{\partial T_w}{\partial r}\right] + \frac{\partial}{\partial x}\left[K_w \frac{\partial T_w}{\partial x}\right] \quad (1)$$

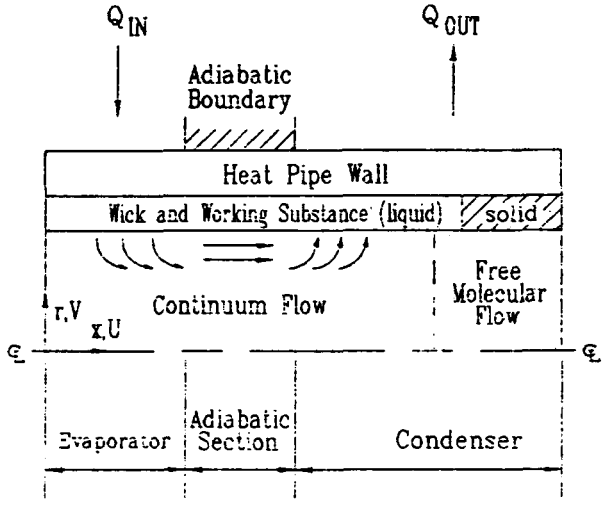

Fig. 1 Schematic diagram and coordinate configuration of the heat pipe.

Wick Structure Region

Initially, the working substance is in the solid state. When heat is added to the evaporator, the frozen working substance in the heated region is melted so that the liquid and solid states of the working substance exist in the wick. Fluid motion in the liquid region may then occur due to vaporization and condensation of the working substance. The liquid flow in the wick is considered to be unsteady two–dimensional incompressible laminar flow with negligible body forces. The fluid and wick structure are assumed to be in local equilibrium and the velocities in the axial and radial directions are the local area–averaged velocities over a cross section of a finite element of the wick region instead of the pore velocity or actual velocity. Also, the wick is assumed to be isotropic and homogeneous. The governing equations for the wick region are formulated by using the principles of the conservation of mass, momentum, and energy. The viscous dissipation terms in the energy equation are neglected.

The continuity, momentum and energy equations are

$$\frac{1}{r}\frac{\partial}{\partial r}(rV_\ell) + \frac{\partial U_\ell}{\partial x} = 0 \quad (2)$$

$$\frac{1}{\epsilon}\frac{\partial V_\ell}{\partial t} + \frac{1}{\epsilon^2}\left[V_\ell \frac{\partial V_\ell}{\partial r} + U_\ell \frac{\partial V_\ell}{\partial x}\right] = -\frac{1}{\rho_\ell}\frac{\partial P_\ell}{\partial r} - \frac{\nu_\ell V_\ell}{k} + \frac{\nu_\ell}{\epsilon}\left[\frac{1}{r}\frac{\partial}{\partial r}\left[r\frac{\partial V_\ell}{\partial r}\right] - \frac{V_\ell}{r^2} + \frac{\partial^2 V_\ell}{\partial x^2}\right] \quad (3)$$

$$\frac{1}{\epsilon}\frac{\partial U_\ell}{\partial t} + \frac{1}{\epsilon^2}\left[V_\ell \frac{\partial U_\ell}{\partial r} + U_\ell \frac{\partial U_\ell}{\partial x}\right] = -\frac{1}{\rho_\ell}\frac{\partial P_\ell}{\partial x} - \frac{\nu_\ell U_\ell}{k} + \frac{\nu_\ell}{\epsilon}\left[\frac{1}{r}\frac{\partial}{\partial r}\left[r\frac{\partial U_\ell}{\partial r}\right] + \frac{\partial^2 U_\ell}{\partial x^2}\right] \quad (4)$$

$$(\rho c_p)_i \frac{\partial T_i}{\partial t} + V_\ell \frac{\partial T_i}{\partial r} + U_\ell \frac{\partial T_i}{\partial x} = \frac{1}{r}\frac{\partial}{\partial r}\left[rK_i \frac{\partial T_i}{\partial r}\right] + \frac{\partial}{\partial x}\left[K_i \frac{\partial T_i}{\partial x}\right] \quad (5)$$

$$i = \begin{cases} se \text{ for solid region} \\ me \text{ for mushy region} \\ \ell e \text{ for liquid region} \end{cases}$$

$$(\rho c_p)_i = \begin{cases} \epsilon(\rho c_p)_{fs} + (1-\epsilon)(\rho c_p)_s \\ \text{for solid region} \\ \epsilon H_{s\ell}\delta(T - T_m) + (1-\epsilon)(\rho c_p)_s \\ \text{for mushy region} \\ \epsilon(\rho c_p)_{f\ell} + (1-\epsilon)(\rho c_p)_s \\ \text{for liquid region} \end{cases} \quad (6)$$

When the porosity approaches unity (no wick structure exists), the permeability approaches infinity. Therefore, equations (2–5) can be reduced to the Navier–Stokes equation for unsteady two–dimensional incompressible laminar flow. For the steady state, equations (2–5) also approach a special case given by Hong et al. (1985). The expressions for the porosity and the effective thermal conductivity of the screen wicks are given by Chang (1987).

The governing equations (2–5), however, are not always applicable. For example, during the second period the liquid state of the working substance exists in the wick but evaporation of the working substance at the interface is negligible. Also, the liquid layer is so thin that the effect of natural convection in the liquid region is neglected. Thus, there is no fluid motion in the liquid region so that only equation (5) without the second and third terms is applicable and equations (2–4) are useful after the second period when there is liquid motion in the wick.

In addition to equations (2–5), coupling conditions at the liquid–solid interface are needed:

$$T_{se} = T_{\ell e} = T_m \quad (7)$$

$$K_{se}\frac{\partial T_{se}}{\partial n} - K_{\ell e}\frac{\partial T_{\ell e}}{\partial n} = \epsilon H_{s\ell}\frac{\vec{dS}}{dt} \quad (8)$$

Vapor flow dynamics

Initially, the entire working substance is in the solid state so that the vapor space may be nearly evacuated. As the temperature at the interface increases, the vapor density also increases. Continuum flow in the vapor space is considered to be established when the mean free path, λ, is substantially less than the mininum dimensions of the vapor flow passage (Holman, 1981), e.g.,

$$K_n \equiv \frac{\lambda}{D} \leq 0.01 \quad (9)$$

The transition temperature, T^*, of the vapor corresponding to the given dimension of the vapor space is expressed by using the kinetic theory of gases as follows (Jang, 1988):

$$T^* \geq \frac{\pi}{2x10^{-4}}\frac{M}{R_u}\left[\frac{\mu_v}{\rho_v D}\right]^2 \quad (10)$$

When the vapor temperature is greater than that calculated by equation (10), continuum flow is assumed to be established in the vapor space.

When continuum flow is established in the vapor space during the start–up from the frozen state, complex flow phenomena are encountered in the continuum flow region due to the extremely small density of the vapor. The vapor pressure is low and the temperature and pressure gradients are large in the axial direction, so the vapor velocity may reach the sonic velocity, and supersonic vapor flow and a shock front may occur in the condenser. Thus, the effects of compressibility, friction at the liquid– vapor interface and dissipation in the vapor should be considered in the mathematical model. The vapor flow may be considered to be axisymmetric, compressible, unsteady laminar flow and the governing equations for this flow are formulated with negligible body forces and heat sources as follows. In cylindrical coordinates, the continuity, momentum and energy equations are:

$$\frac{\partial \rho_v}{\partial t} + \frac{1}{r}\frac{\partial}{\partial r}(r\rho_v V_v) + \frac{\partial(\rho_v U_v)}{\partial x} = 0 \quad (11)$$

$$\rho_v\left[\frac{\partial V_v}{\partial t} + V_v\frac{\partial V_v}{\partial r} + U_v\frac{\partial V_v}{\partial x}\right] = -\frac{\partial P_v}{\partial r} + \mu_v\left[\frac{4}{3}\frac{\partial}{\partial r}\left[r\frac{\partial V_v}{\partial r}\right] - \frac{4}{3}\frac{V_v}{r^2} + \frac{1}{3}\frac{\partial^2 U_v}{\partial x \partial r} + \frac{\partial^2 V_v}{\partial x^2}\right] \quad (12)$$

$$\rho_v\left[\frac{\partial U_v}{\partial t} + U_v\frac{\partial V_v}{\partial r} + U_v\frac{\partial U_v}{\partial x}\right] = -\frac{\partial P_v}{\partial x} + \mu_v\left\{\frac{1}{r}\frac{\partial}{\partial r}\left[r\left[\frac{\partial V_v}{\partial x} + \frac{\partial U_v}{\partial r}\right]\right] - \frac{2}{3}\frac{\partial}{\partial x}\left[\frac{1}{r}\frac{\partial}{\partial r}(rV_v)\right] + \frac{4}{3}\frac{\partial}{\partial x}\left[\frac{\partial U_v}{\partial x}\right]\right\} \quad (13)$$

$$\rho_v C_{pv}\left[\frac{\partial T_v}{\partial t} + V_v\frac{\partial T_v}{\partial r} + U_v\frac{\partial T_v}{\partial x}\right] = \frac{1}{r}\frac{\partial}{\partial r}\left[rK_v\frac{\partial T_v}{\partial r}\right] + \frac{\partial}{\partial x}\left[K_v\frac{\partial T_v}{\partial x}\right] + \frac{\partial P_v}{\partial t} + V_v\frac{\partial P_v}{\partial r} + U_v\frac{\partial P_v}{\partial x} + \mu_v\phi \quad (14)$$

Where:

$$\phi = 2\left[\left[\frac{\partial V_v}{\partial r}\right]^2 + \left[\frac{V_v}{r}\right]^2 + \left[\frac{\partial U_v}{\partial x}\right]^2 + \frac{1}{2}\left[\frac{\partial V_v}{\partial r} + \frac{\partial U_v}{\partial r}\right]^2 - \frac{1}{3}(\nabla \cdot V)^2\right] \quad \nabla \cdot V = \frac{1}{r}\frac{\partial}{\partial r}(rV_v) + \frac{\partial U_v}{\partial x}$$

The numerical and analytical solutions of the above equations under steady state conditions for annular and conventional heat pipes were given by Faghri (1986) and Faghri and Parvani (1988). Transient results are needed for the start–up from the frozen condition.

Initial and Boundary Conditions

Initially, a uniform temperature for the wall, wick, and vapor regions is assumed which is less than the melting temperature of the working substance. So, the entire working substance in the wick is in the solid state. The heat flux, convection and radiation boundary conditions are applicable at the outer surface of the evaporator and condenser of the heat pipe. Both ends of the heat pipe are assumed to be insulated. When the liquid motion exists in the wick structure, the no–slip condition is used for the velocities at the interface between the heat pipe wall and the wick structure.

The boundary conditions at the liquid–vapor interface change during the start–up process. In the first and second periods, free molecular flow is prevalent in the

vapor space so that heat transfer through the vapor space is negligible. Therefore, the adiabatic condition is employed at the liquid–vapor interface. When continuum flow is established in the vapor space, vaporization and condensation of the working substance at the interface is considered by using interface energy and mass balances. The vapor temperature at the interface is assumed to be the saturation temperature corresponding to the vapor pressure at the interface. The Clausius–Clapeyron relationship is used to obtain the saturation temperature. The continuity of the axial velocity and shear stress is also used. The pressure difference at the liquid–vapor interface induced from the action of the surface tension is given by using the Laplace and Young equation. This condition couples the liquid and vapor momentum equations at the liquid–vapor interface.

While part of the vapor space is in the continuum flow regime, free molecular flow also exists in the rest of the vapor space. Even though the heat transfer through the free molecular flow region may be negligible, the boundary conditions at the border of the two regions are needed to solve the governing equations for the continuum flow region. Since a large temperature gradient exists in the continuum flow region in the condenser during start–up, most of the vapor may be condensed at the interface. Thus, the vapor penetration in the free molecular flow region may be minimal or penetration may occur in the immediate vicinity of the interface between the continuum flow region and the free molecular flow region. Also, the temperature in the region of free molecular flow remains unchanged except in the vicinity of the continuum flow region due to the near vacuum. Therefore, an imaginary plane, which is adiabatic and normal to the axial direction, is assumed to divide the two vapor flow regions at the point of the transition temperature. The dividing plane moves towards the cooled end of the heat pipe as the location of the transition temperature at the liquid–vapor interface moves.

The axisymmetric condition along the centerline of the heat pipe is used in continuum flow region. The no–slip condition and the adiabatic condition at both ends of the heat pipe is also used for the velocities and temperature. The pressure and density at both ends of the heat pipe are unknown but the vapor velocity near the ends of the heat pipe is so low that the axial pressure and density gradients are assumed to be zero. All of the boundary conditions for a mathematical model of the heat pipe start–up from the frozen state is summarized in Table 1.

SIMPLIFICATION OF THE MODEL

The mathematical model, equations (1–14), for the start–up behavior of the liquid metal heat pipe described in the previous section includes most of the physical phenomena which may occur in the heat pipe. Therefore, this model is very complex to solve numerically. The effect of some physical phenomena may be negligible, so a simplified model is derived to predict the performance of the heat pipe during the start–up period. For this purpose, assumptions are made based on the characteristics of the heat pipe and previous studies.

The density of the liquid state of the working substance is much greater than that of the vapor state, so the velocity of the working substance in the wick structure is small. The thermal conductivity of the liquid metal is large and the thickness of the wick region is very thin. It is then assumed that the effect of the liquid flow in the wick structure is negligible and the wick structure is saturated by the working substance. Thus, the heat transport through the wick structure and working substance is by conduction only but the phase change of the working substance is considered. Under these assumptions, the same governing equation is also applicable to the heat pipe wall and the wick structure by using the proper properties for each region. The governing equation is given as follows:

$$(\rho c_p)_i \frac{\partial T_i}{\partial t} = \frac{1}{r}\frac{\partial}{\partial r}\left[rK_i \frac{\partial T_i}{\partial r}\right] + \frac{\partial}{\partial x}\left[K_i \frac{\partial T_i}{\partial x}\right] \tag{15}$$

$$i = \begin{cases} w & \text{for wall region} \\ se & \text{for solid region in the wick} \\ me & \text{for mushy region in the wick} \\ \ell e & \text{for liquid region in the wick} \end{cases}$$

The expression of $(\rho c_p)_i$ for the wick structure region is given by equation (6). The thermal conductivity, K_i, can be the thermal conductivity of the wall material for the wall region. When the effective thermal conductivity for the wick region is calculated by using the expression given by Chang (1987), the thermal conductivity for the working substance is substituted by the solid conductivity, liquid conductivity, or the average value of the solid and liquid conductivity of the working substance corresponding to the solid, liquid, or mushy region, respectively.

The vapor flow is also simplified further from the two–dimensional model to a one–dimensional model since a previous study (Jang et al., 1989) shows that the one–dimensional transient compressible model described the vapor flow dynamics as well as the two–dimensional model for simulated heat pipe vapor flow. The transient compressible one–dimensional continuity, momentum and energy equation are written as follows:

$$\frac{\partial}{\partial t}(\rho_v) + \frac{\partial}{\partial x}(\rho U_v) = \frac{4\rho_o V_o(x)}{D} \tag{16}$$

$$\frac{\partial}{\partial t}(\rho_v U_v) + \frac{\partial}{\partial x}(\rho_v U_v U_v) + \frac{\partial}{\partial x}\left[P_v - \frac{4}{3}\mu_v \frac{\partial U_v}{\partial x}\right] = -\frac{2\rho_v U_v^2 f}{D} \tag{17}$$

$$\frac{\partial E_v}{\partial t} + \frac{\partial}{\partial x}\left[U_v(E_v + P_v) - \frac{4}{3}\mu_v \frac{\partial U_v}{\partial x} U_v - K_v \frac{\partial T_v}{\partial x}\right] = \frac{4\rho_o V_o(x)}{D}\left[h_o(x) + \frac{V_o^2(x)}{2}\right] + \frac{2\rho_v U_v^2 f}{D} U_v \tag{18}$$

Since the governing equations are simplified, the corresponding boundary conditions are also modified to match the governing equations.

NUMERICAL PROCEDURES

The governing equations are separately solved for each region. When the coupling is implemented at the interface, iterations are needed. To reduce the amount of computer time, non–iterative schemes are employed for each region. The well–known alternating direction implicit (ADI) method is used for the heat pipe wall and wick, and the phase change of the working substance during start–up is modeled by using the equivalent heat capacity method (Hsiao, 1985). This method approximates the rapid change of the heat capacity over the phase change temperature range, which is an artificially defined finite temperature range, ΔT, instead of using the Dirac function. In the numerical calculation, this property is evaluated based on the nodal temperatures. The implicit Beam–Warming method is used for the vapor flow dynamics. The detailed numerical method for the vapor flow in the heat pipe is described by Jang et al. (1989).

After continuum flow exists in the vapor space, equation (15) should be coupled with equations (16–18) by using the same boundary conditions at the interface. The coupling of the governing equations for the vapor region to those for the wall and wick regions would be achieved by using the heat flux and the saturation temperature at the interface. However, the heat flux at this interface and the saturation temperature are initially unknown, so that these boundary conditions should be assumed and iterations are needed for each time step until the coupling conditions are satisfied along the interface. The numerical procedure used for coupling is as follows:

1. It is assumed that the liquid–vapor interface temperature is the initial temperature for the first time step.
2. Solve for the temperatures in the wall and wick regions.
3. Calculate the heat fluxes, q, at each node of the liquid–vapor interface by using the temperatures (T_{j-1} and T_j) in the wick region.

$$q = K_{\ell e} \frac{(T_{j-1} - T_j)}{\Delta r} \qquad (19)$$

4. These heat fluxes are used as the boundary conditions at the interface to solve for temperatures in the wall and wick regions.
5. Use the same heat fluxes to solve the vapor temperature and pressure for the same period at the wall and wick regions. Obtain the saturation temperature, T_s, by using the Clausius–Clapeyron relationship.
6. Calculate the new heat fluxes, q′, at the interface by using the saturation temperature, T_s, in the wick.

$$q' = K_{\ell e} \frac{(T_{j-1} - T_s)}{1.5\Delta r} \qquad (20)$$

7. Compare the new heat fluxes, q′, with the old heat fluxes, q, at each node of the interface.
8. If the difference between the new heat flux and old heat flux is within an acceptable range, repeat steps 4 to 7 for the next time step.
9. If the difference between the new heat flux and the old heat flux is not within the acceptable range, assume new guessed heat fluxes, q", by using the relaxation method and repeat steps 4 to 7 until the comparison of the results is acceptable.

$$q'' = q + \alpha (q' - q) \qquad (21)$$

10. Repeat steps 4 to 9 until the temperatures reach the steady state.

When the coupling of the governing equations is attempted, some physical characteristics of the two regions are considered. Since the density of the vapor is much smaller than that of the liquid, the volumetric specific heat ρc_p (= 8.8 J/m^{3}K) for the vapor is much smaller than that (= 1040.1 KJ/m^{3}K) for the liquid. Therefore, a difference between the transient response times of the vapor region, and the wall and wick regions exists. The time step for the vapor space should then be much smaller than that for the wall and wick regions. The governing equations for the wall and wick regions are solved for one time step by using the heat flux assumed at the interface, and then the governing equations for the vapor space are solved by using the same heat flux at the interface and smaller time steps for the same period as the wall and wick regions.

RESULTS AND DISCUSSION

The governing equations for the wall and wick regions and the vapor flow are separately solved, and then are coupled at the liquid–vapor interface. Therefore, the numerical methods and algorithms can be separately tested and compared to the available data. Since the working substance changes phase from the solid state to the liquid state during the start–up period from the frozen state, this effect should be incorporated into the numerical model. The solidification of sodium in a square region is chosen to verify the numerical model and algorithm for governing equation (15). The results are in agreement with available data (Rathjen and Jiji, 1971). The transient one–dimensional model for the vapor flow dynamics in the heat pipe has already been verified by Jang et al. (1989). The combined model is used to predict the performance of the liquid–metal heat pipe.

Simulation of the heat pipe start–up in the initial stages

Previous experimental results (Deverall et al., 1970) show that successful start–up of the frozen heat pipe greatly depends on the boundary condition at the outer surface of the evaporator and condenser. For successful start–up from the frozen state, the heat input and output should melt the working substance in the condenser and allow sufficient liquid to return to the evaporator. All of the previous experimental results show the wall surface temperatures, so that even for successful start–up the status of the working substance with time is unknown. Thus, the governing equations which described the start–up behavior of a cylindrical heat pipe during the first and second periods are solved numerically to examine the effect of the boundary conditions and to recommend the optimum boundary condition.

The physical model has evaporator, adiabatic, and condenser section lengths of 0.2, 0.1 and 0.2 m, respectively. The radius of the vapor space and the inner and outer radii of the heat pipe wall are 0.00685, 0.008, and 0.01 m, respectively. The material for the heat pipe wall and wick structure is stainless steel (AISI 316). Sodium initially in the solid state at the ambient temperature is used as the working substance. The melting temperature of sodium is 371 K and the transition temperature of 680 K is obtained by using equation (10) for the radius of the vapor space (0.00685m) by iteration. Three different boundary condition cases are chosen for the outer surface of the heat pipe. A uniform input heat flux of 50 KW/m^2 and radiative heat output are used on the evaporator for all three cases. An emissivity of 0.9 and a radiation reference temperature of 293 K are employed. The boundary conditions at the condenser and adiabatic sections are changed while that at the evaporator remains the same for all three cases. The liquid–vapor interface is assumed to be adiabatic due to the free molecular flow in the vapor space during initial two periods.

For case 1, only radiation is used in the condenser to reject heat. Figure 2 shows the temperature distributions at the heat pipe outer wall surface and the liquid–vapor interface. As heat is added in the evaporator, the temperature in the evaporator increases and at 20 seconds the working substance in the evaporator is in the liquid state. However, the temperature in the condenser is not changed from the initial temperature and in the adiabatic section the temperature in the region adjacent to the evaporator increases due to axial conduction. Additional heat input in the evaporator increases the temperature above the transition temperature in the evaporator, but the temperature in the condenser is still not changed so that a large temperature gradient exists. In the adiabatic section, part of the working substance (sodium) is in the liquid

state. When the heat input is continued at the evaporator, vaporization occurs at the interface in the evaporator. However, the working substance in most of the adiabatic section and condenser is in the solid state. Therefore, the heat input in the evaporator should be small to prevent dry–out of the wick structure while the working substance in the solid state is melted. Even though successful start–up may be possible for this case, the start–up progresses very slowly.

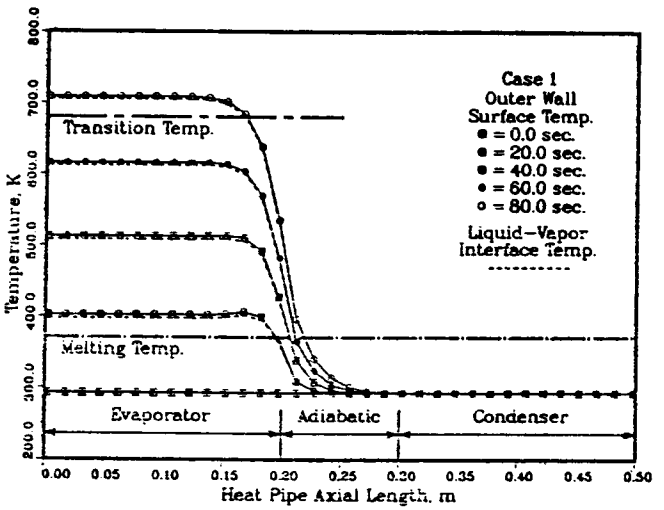

Fig. 2 Temperature distribution at the outer wall surface and liquid–vapor interface of the heat pipe wall with time for case 1.

For case 2, 10 kW/m^2 is added in the condenser in addition to the radiative boundary condition to assist in the start–up of the frozen heat pipe. Figure 3 shows the temperature distributions at the outer wall surface and liquid–vapor interface. Since a small amount of heat is added in the condenser, the temperature in the condenser is raised above the melting temperature. However the temperature in the adiabatic section is still below the

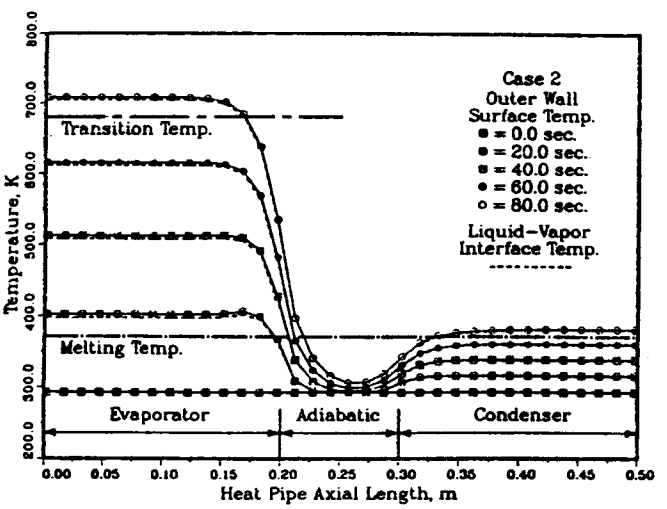

Fig. 3 Temperature distribution at the outer wall surface and liquid–vapor interface of the heat pipe wall with time for case 2.

melting temperature. Thus, liquid in the condenser cannot flow to evaporator until the working substance in the adiabatic section liquefies. The temperature in the adiabatic section increases relatively faster than that for case 1 due to heat transfer at both ends of the adiabatic section. The start–up period may be shorter than that for case 1.

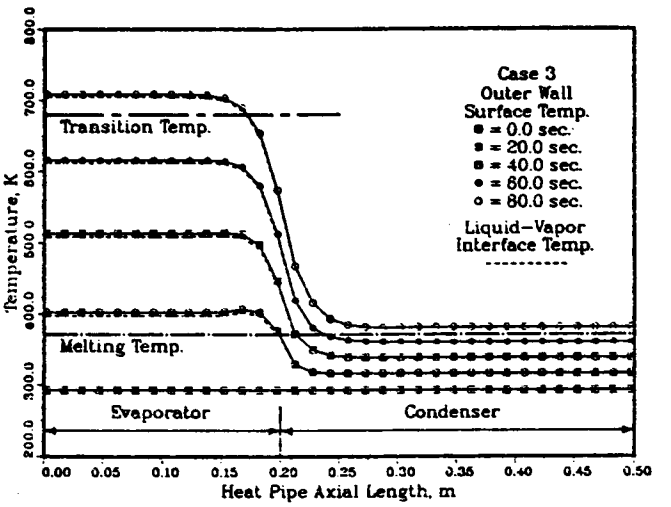

Fig. 4 Temperature distribution at the outer wall surface and liquid–vapor interface of the heat pipe wall with time for case 3.

Finally, the adiabatic section is used as part of the condenser and 10 kW/m^2 of heat is input in the condenser section. Figure 4 shows the temperature distributions at the heat pipe surface and the liquid–vapor interface and Fig. 5 shows the surface temperature at different times. Even though a large temperature gradient still exists along the axial direction, the working substance is completely melted in the entire heat pipe in 80 seconds. When vaporization occurs in the evaporator, the working substance can flow from the condenser to the evaporator to prevent dry–out of the wick structure in the evaporator. Thus, a relatively large amount heat can be added at the evaporator without dry–out so that the start–up period is expected to be much less than those of cases 1 and 2.

Transient Heat Pipe Operation

To simulate the coupling of the governing equation for the wall and wick to that for the vapor flow, the same physical heat pipe model is used except that the adiabatic section is eliminated. Sodium is employed as the working substance. In order to concentrate on the coupling problem, it is assumed that continuum flow is established in the entire vapor space and the working substance is in the liquid state. To yield these conditions, a uniform initial temperature of 800 K, which is greater than the transition temperature (680 K), is used for the wall, wick, and vapor regions. The external surfaces of the heat pipe wall at the evaporator and condenser are exposed to a uniform heat flux of 50000 W/m^2 and a convective boundary condition, respectively. A reference temperature of 300 K and a heat transfer coefficient of 100 W/m^2K are used for the convective boundary condition at the condenser section. The time step for the vapor space should be much smaller than that for the wall and wick regions, so a time step of 0.1

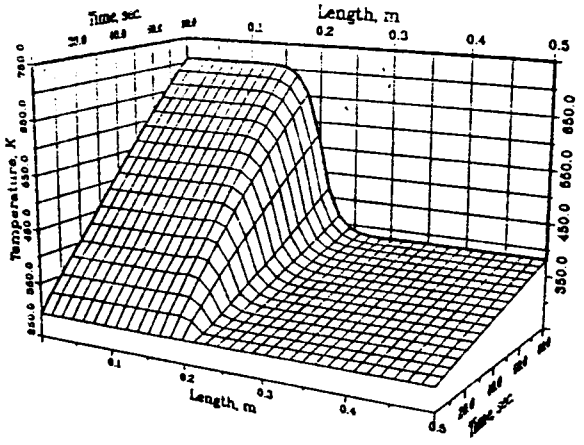

Fig. 5 Temperature distribution at the outer wall surface of the heat pipe wall with different times for case 3.

second is employed for the wall and wick regions and time step of 0.1×10^{-3} second is used for the vapor flow. Twenty nodes in the radial direction and 160 nodes in the axial direction are used at the wall and wick regions. Also, 160 nodes are employed along the vapor space. A relaxation factor of $\alpha = 0.00003$ is used to obtain the new guessed heat flux.

Figure 6 shows the temperature distributions at the outer wall surface, liquid–vapor interface, and the saturation temperature for a time of 0.3 second. The temperature distribution at the outer wall surface is uniform within each section, and near the border between the evaporator and condenser the surface temperature abruptly changes corresponding to the boundary conditions at the surface. The interface temperature matches well with the

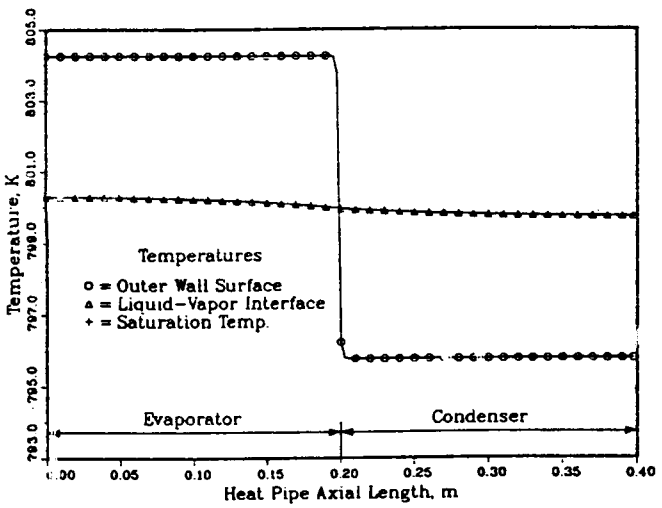

Fig. 6 Temperature distributions at the outer wall surface and liquid–vapor interface, and saturation temperature for time of 0.3 second.

saturation temperature which is evaluated by using the Clausius–Clapeyron relationship with the vapor pressure. The saturation temperature decreases gradually. Figure 7 shows the heat flux distribution at the interface. The new heat flux calculated is converged to the old heat flux. The maximum difference between the two heat fluxes is about 10%. Even though the heat flux at the surface is relatively uniform, the heat flux at the interface is not uniform. Also, the heat flux at the interface is much less than that at the surface. This implies that most of the energy is used to raise the wall and wick temperature at this moment. Figure 8 shows the vapor temperature, pressure, velocity, and density distributions. The variation of the vapor temperature,

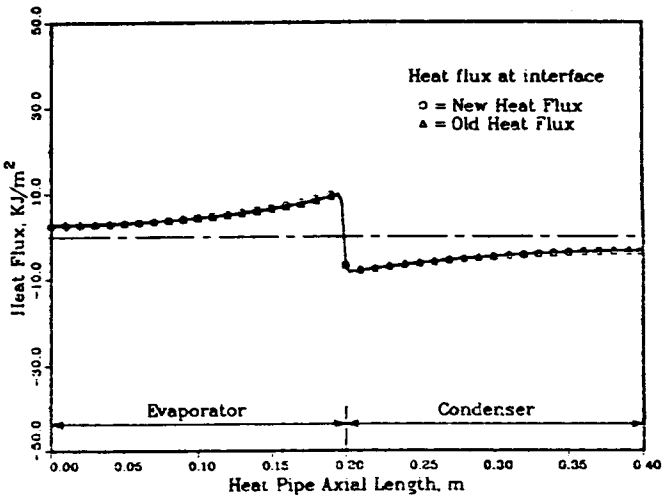

Fig. 7 Comparison of new heat flux with old heat flux at the interface for time of 0.3 second during transient continuum flow.

pressure, and density is small. Also, a Mach number of M = 0.027 is obtained at the exit of the evaporator.

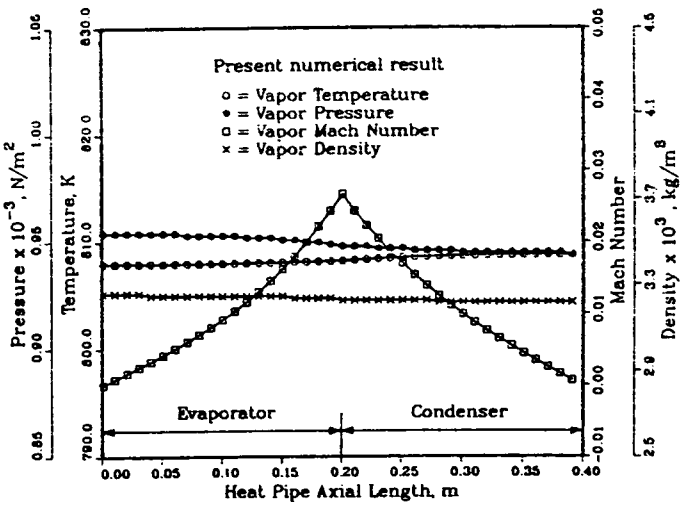

Fig. 8 Axial variations of temperature, pressure, density and velocity for time of 0.3 second during transient continuum flow.

CONCLUSIONS

The start–up process of the frozen heat pipe is

described based on the experimental results. A complete mathematical model is developed to predict the start–up behavior of the heat pipe from the frozen condition. The simplified model is used to obtain the numerical results. The numerical results during the first and second periods show that the heat flux distributions for the evaporator and condenser should be chosen to melt the working substance in the condenser prior to vaporization occurring in the evaporator. A small amount of heat input at the condenser helps start–up and a high heat rejection at the condenser during the start–up should be avoided. The coupling of the two–dimensional transient model for the wall and wick to the one–dimensional transient model for the vapor flow is achieved when continuum flow exists in the vapor space. During the transient operation, the heat flux distribution at the interface is quite different from that at the surface. Efforts to improve the present model will continue.

ACKNOWLEDGEMENT

Funding for this work was provided by a joint effort of the NASA Lewis Research Center and the Thermal Energy Group of the Aero Propulsion and Power Laboratory of the U.S. Air Force under contract F33615–88–C–2820.

REFERENCES

Camarda, C.J., 1977, "Analysis and Radiant Heating Tests of a Heat–Pipe– Cooled Leading Edge," NASA TN–8486.

Chang, W.S., 1987, "Effective Thermal Conductivity of Wire Screens," Fundamentals of Conduction and Recent Developments in Contact Resistance, HTD–Vol. 69, pp. 64–75.

Colwell, G.T., Jang, J.H., and Camarda, C.J., 1987, "Modeling of Startup from the Frozen State," Proc. 6th Int. Heat Pipe Conf., France. Vol. 1, pp. 165–170.

Cotter, T.P., 1967, "Heat Pipe Startup Dynamics," Proc. IEEE Thermionic Conversion Specialist Conf., Palo Alto Calif., pp. 344–348.

Deverall, J.E., Kemme, J.E., and Florschuetz, L.W., 1970, "Sonic Limitations and Startup Problems of Heat Pipes," LA–4518.

Dunn, P.D., and Reay, D.A., 1982, Heat Pipes, 3rd Ed., Pergamon Press, Oxford.

Faghri, A., 1986, "Vapor Flow Analysis in a Double–Walled Concentric Heat Pipe," Numerical Heat Transfer, Vol. 10, No. 6, pp. 583–595.

Faghri, A., and Parvani, S., 1988, "Numerical Analysis of Laminar Flow in a Double–Walled Heat Pipe," J. Thermophysics and Heat Transfer, Vol. 2, No. 3, pp. 165–171.

Holman, J.P., 1981, Heat Transfer, 5th Ed., McGraw–Hill Book Co., New York.

Hong, J.T., Tien, C.L., and Kaviany, M., 1985, "Non–Darcian Effects on Vertical–Plate Natural Convection in Porous Media with High Porosities," Int. J. Heat Mass Transfer, Vol. 28, pp. 2149–2157.

Hsiao, J.S., 1985, "An Efficient Algorithm for Finite–Difference Analysis of Heat Transfer with Melting and Solidification," Numerical Heat Transfer, Vol. 8, pp. 653–666.

Ivanovskii, M.N., Sorokin, V.P., and Yagodkin, I.V., 1982, The Physical Principles of Heat Pipes, Clarendon Press, Oxford.

Jang, J.H., 1988, "An Analysis of Startup from the Frozen State and Transient Performance of Heat Pipes," Ph.D. Dissertation, Georgia Institute of Technology.

Jang, J.H., Faghri, A., and Chang, W.S., 1989, "Analysis of the Transient Compressible Vapor Flow in Heat Pipes," Proc. of 26th National Heat Transfer Conf, Philadephia, Pennsylvania.

Merrigan, M.A., Keddy, E.S., and Sena, J.T., 1985, "Transient Heat Pipe Investigations for Space Power Systems," LA–UR–85–3341.

Merrigan, M.A., Keddy, E.S., and Sena, J.T., 1986, "Transient Performance Investigation of a Space Power System Heat Pipe," AIAA Paper No. AIAA–86–1273.

Neal, L.G., 1967, "An Analysis and Experimental Study of Heat Pipes," TRW System Rept. No. 99900–6114–R000.

Rathjen, K.A., and Jiji, L.M., 1971, "Heat Conduction with Melting or Freezing in a Corner," J. Heat Transfer, Vol. 93, pp. 101–109.

Shlosinger, A.P., 1968, "Heat Pipe Devices for Space Suit Temperature Control," TRW System Rept. No. 06462–6005–RO–00.

Tolubinsky, V.I., Shevchuk, E.N., and Stambrovsky, V.D., 1978, "Study of Liquid–Metal Heat Pipes Characteristics at Start–up and Operation under Gravitation," Proc. of 3rd Int. Heat Pipe Conf., pp. 274–282.

Table 1. Summary of the boundary conditions for a mathematical model of the heat pipe start-up

Time	1st and 2nd periods	3rd period	4th period	5th and 6th periods
Event	heat transfer by conduction; no liquid motion; free molecular flow	solid and liquid states; liquid motion in the wick; continuum flow in the part of the vapor space	no solid state of the working substance; liquid motion in the wick; continuum flow in the part of the vapor space	liquid motion in the wick; continuum flow in the entire vapor space; the heat pipe approaches the steady state operation
Location				
outer wall surface	$K_w \frac{\partial T_w}{\partial r} = q(x,t) + h_c(T_c - T_w) + \sigma\xi(T_r^4 - T_w^4)$			
wall and wick structure interface ($r = R_w$)	$T_w = T_i$ $K_w \frac{\partial T_w}{\partial r} = K_i \frac{\partial T_i}{\partial r}$	$T_w = T_i$ $K_w \frac{\partial T_w}{\partial r} = K_i \frac{\partial T_i}{\partial r}$ $U_\ell = V_\ell = 0$ for $T_i > T_m$ (liquid region)	$T_w = T_{\ell e}$ $K_w \frac{\partial T_w}{\partial r} = K_{\ell e} \frac{\partial T_{\ell e}}{\partial r}$ $U_\ell = V_\ell = 0$	
liquid-vapor interface ($r = R_v$)	$\frac{\partial T_i}{\partial r} = 0$	$\frac{\partial T_i}{\partial r} = 0$ for $T_i < T^*$ (free molecular flow region) $K_{\ell e} \frac{\partial T_{\ell e}}{\partial r} - K_v \frac{\partial T_v}{\partial r} = h_{\ell v} \dot{m}_o$ for $T_{\ell e} \geq T^*$ $U_\ell = U_v$, $\mu_\ell \frac{\partial U_\ell}{\partial r} = \mu_v \frac{\partial U_v}{\partial r}$ $V_\ell = -\frac{B\dot{m}_o}{\rho_\ell} = \frac{\rho_v}{\rho_\ell} V_v$ $P_v - P_\ell = \frac{2\sigma}{r_p}$ $T_s = \frac{1}{\frac{1}{T_{cr}} - \frac{R_u}{Mh_{\ell v}} \ell n \frac{P}{P_{cr}}}$	$\frac{\partial T_{\ell e}}{\partial r} = 0$ for $T_{\ell e} < T^*$ (free molecular flow region) $K_{\ell e} \frac{\partial T_{\ell e}}{\partial r} - K_v \frac{\partial T_v}{\partial r} = h_{\ell v} \dot{m}_o$ for $T_{\ell e} \geq T^*$ $U_\ell = U_v$, $\mu_\ell \frac{\partial U_\ell}{\partial r} = \mu_v \frac{\partial U_v}{\partial r}$ $V_\ell = -\frac{B\dot{m}_o}{\rho_\ell} = \frac{\rho_v}{\rho_\ell} V_v$ $P_v - P_\ell = \frac{2\sigma}{r_p}$ $T_s = \frac{1}{\frac{1}{T_{cr}} - \frac{R_u}{Mh_{\ell v}} \ell n \frac{P}{P_{cr}}}$	$K_{\ell e} \frac{\partial T_{\ell e}}{\partial r} - K_v \frac{\partial T_v}{\partial r} = h_{\ell v} \dot{m}_o$ $U_\ell = U_v$ $\mu_\ell \frac{\partial U_\ell}{\partial r} = \mu_v \frac{\partial U_v}{\partial r}$ $V_\ell = -\frac{B\dot{m}_o}{\rho_\ell} = \frac{\rho_v}{\rho_\ell} V_v$ $P_v - P_\ell = \frac{2\sigma}{r_p}$ $T_s = \frac{1}{\frac{1}{T_{cr}} - \frac{R_u}{Mh_{\ell v}} \ell n \frac{P}{P_{cr}}}$
both ends of the pipe ($x = 0, L$) — wall	$\frac{\partial T_w}{\partial x} = 0$			
both ends of the pipe ($x = 0, L$) — wick structure	$\frac{\partial T_i}{\partial x} = 0$	$\frac{\partial T_i}{\partial x} = 0$ $U_\ell = V_\ell = 0$ for $T_i > T_m$ (liquid region)	$\frac{\partial T_{\ell e}}{\partial x} = 0$ $U_\ell = V_\ell = 0$	
both ends of the pipe ($x = 0, L$) — vapor space	no boundary condition is needed due to free molecular flow	$U_v = V_v = 0$ for $T_{\ell e} \geq T^*$ (continuum flow region) $\frac{\partial T_v}{\partial x} = \frac{\partial P_v}{\partial x} = \frac{\partial \rho_v}{\partial x} = 0$		$U_v = V_v = 0$ $\frac{\partial T_v}{\partial x} = \frac{\partial P_v}{\partial x} = \frac{\partial \rho_v}{\partial x} = 0$
centerline of the pipe ($r = 0$)	no boundary condition is needed due to free molecular flow	$V_v = 0$ for $T_{\ell e} \geq T^*$ (continuum flow region) $\frac{\partial \rho_v}{\partial r} = \frac{\partial U_v}{\partial r} = \frac{\partial E_v}{\partial r} = \frac{\partial P_v}{\partial r} = 0$		$V_v = 0$ $\frac{\partial \rho_v}{\partial r} = \frac{\partial U_v}{\partial r} = \frac{\partial E_v}{\partial r} = \frac{\partial P_v}{\partial r} = 0$

NASA
National Aeronautics and Space Administration

Report Documentation Page

1. Report No.	2. Government Accession No.	3. Recipient's Catalog No.
NASA CR-185132		

4. Title and Subtitle
Mathematical Modeling and Analysis of Heat Pipe Start-Up From From the Frozen State

5. Report Date
August 1989

6. Performing Organization Code

7. Author(s)
Jong Hoon Jang, Amir Faghri, Won Soon Chang, and Edward T. Mahefkey

8. Performing Organization Report No.
None (E-5028)

10. Work Unit No.
586-01-21

9. Performing Organization Name and Address
Wright State University
Department of Mechanical Systems Engineering
Dayton, Ohio 45435

11. Contract or Grant No.

13. Type of Report and Period Covered
Contractor Report
Final

12. Sponsoring Agency Name and Address
National Aeronautics and Space Administration
Lewis Research Center
Cleveland, Ohio 44135-3191

14. Sponsoring Agency Code

15. Supplementary Notes
Project Manager, Albert J. Juhasz, Power Technology Division, NASA Lewis Research Center; Jong Hoon Jang and Amir Faghri, Dept. of Mechanical Systems Engineering, Dayton, Ohio 45435; Won Soon Chang and Edward T. Mahefkey, Wright Research and Development Center, Wright-Patterson AFB, Ohio 45433 (work funded by Air Force Contract F336 15-88-C-2820). Jong Hoon Jang, presently with Sverdrup Technology, Inc., NASA Lewis Research Center Group, Cleveland, Ohio 44135. Prepared for the 1989 Annual Winter Meeting of the American Society of Mechanical Engineers, San Francisco, California, December 10-15, 1989.

16. Abstract
The start-up process of a frozen heat pipe is described and a complete mathematical model for the start-up of the frozen heat pipe is developed based on the existing experimental data, which is simplified and solved numerically. The two-dimensional transient model for the wall and wick is coupled with the one-dimensional transient model for the vapor flow when vaporization and condensation occur at the interface. A parametric study is performed to examine the effect of the boundary specification at the surface of the outer wall on the successful start-up from the frozen state. For successful start-up, the boundary specification at the outer wall surface must melt the working substance in the condenser before dry-out takes place in the evaporator.

17. Key Words (Suggested by Author(s))	18. Distribution Statement
Heat pipe; Frozen state; Start-up; Transient; Phase change	Unclassified - Unlimited Subject Category 34

19. Security Classif. (of this report)	20. Security Classif. (of this page)	21. No of pages	22. Price*
Unclassified	Unclassified	12	A03

NASA FORM 1626 OCT 86

*For sale by the National Technical Information Service, Springfield, Virginia 22161